GDCh Research Article Angewandte International Edition Chemie www.angewandte.org

How to cite: *Angew. Chem. Int. Ed.* **2025**, *64*, e202504564
doi.org/10.1002/anie.202504564

Fluorescent Probes

Redox-Activated Near Infrared/Shortwave Infrared Emissive Chromophores: Synthesis of Triphenylamine-Appended Pyrazinacenes

Gary J. Richards, Kazushi Nakada, Keita Aoki, Tomoki Jitsukata, Kana Hashimoto, Toshiki Tajima, Ryusuke Mizoguchi, Ayumi Ishii, Jonathan P. Hill,* and Akiko Hori**

Abstract: Organic dyes showing absorbance and fluorescence in the near infrared and short-wave infrared regions are attractive for a variety of applications. Redox-coupled reversible switching of absorbance or fluorescence implies enhanced functionality of such dyes, especially where large changes in photophysical properties across the redox process can be realized. Here, the synthesis of two new pyrazinacenes containing four and five fused pyrazine units, appended with electron-donor triphenylamine groups, and redox-coupled switching of their photophysical properties is reported. In their reduced state, the compounds show absorbance and fluorescence in the visible region. Reversible shifts in absorbance and fluorescence from the visible to the near infrared or even short-wave infrared regions are observed upon chemical and electrochemical oxidations. Such large redox-coupled shifts in photophysical properties are unprecedented for a redox process that affects only a single, six-membered ring in which both reduced and oxidized states consist of neutral, closed-shell species. The compounds show high fluorescence quantum yields in their reduced states, and oxidized species show fluorescence quantum yields that compare well with existing near infrared and short-wave infrared active fluorescent dyes.

Introduction

NIR and short-wave infrared (SWIR) dyes have attracted significant interest due to potential applications in a wide variety of nascent technologies. Strong absorption and fluorescence in the NIR region are both attractive properties, where NIR emission is important in bioimaging,[1–4] NIR light emitting diodes,[5–7] or for microscopy staining.[8–10] Strong NIR absorption is required for dye-sensitized solar cells,[11–13] sensitizers, and contrast agents for photoacoustic tomography,[14–16] laser-protecting glasses,[17,18] or for NIR absorbing paints and windows.[19,20] Redox-coupled reversible switching of absorbance or fluorescence also implies enhanced functionality in optical switching devices[21–23] or as probes[24,25] of biological redox processes.[26–28] For many applications, large redox-coupled shifts in absorption or fluorescence are advantageous. For example, optical switching and photonic devices often rely on well-separated absorption or fluorescence bands between switched states. Detection of redox imbalance in biological samples using redox-active fluorescent probes is facilitated when the oxidized and reduced species have very different absorption and fluorescence characteristics. Fluorescent redox sensors can operate in the preferred ratiometric mode when the fluorescence spectra of reduced and oxidized species are well separated. Various redox-active dyes have been developed[27–29] with most examples having activity in the NIR/SWIR regions being cyanine dyes, which can suffer from poor photostability or low fluorescence quantum yields.[30,31] Thus, the development of new types of redox-active dyes with activity in the NIR region remains an important goal.

Pyrazinacenes[32–34] (Scheme 1a,b) consist of rectilinearly fused pyrazine units and are highly nitrogenated counterparts of C─H acenes (fused benzenes). In contrast to the relatively electron-rich acenes, which are increasingly prone to oxidation with increasing length, higher analogs of pyrazinacenes are increasingly electron-deficient so they tend to exist containing a reduced dihydropyrazine unit.[35] Despite this, pyrazinacenes with 4 or 5 pyrazine units can undergo reversible redox processes between a highly electron-deficient pyrazine-only oxidized state and a reduced species with a single dihydropyrazine unit.[36] However, before this work, redox-active pyrazinacenes only showed small redox-coupled shifts (typically < 100 nm) in absorption and fluorescence

[*] G. J. Richards, K. Nakada, K. Aoki, T. Jitsukata, A. Hori
Department of Applied Chemistry, Graduate School of Engineering and Science, Shibaura Institute of Technology, Fukasaku 307, Minuma-ku, Saitama 337-8570, Japan
E-mail: richards@shibaura-it.ac.jp
ahori@shibaura-it.ac.jp

K. Hashimoto, T. Tajima
Department of Applied Chemistry, Graduate School of Engineering and Science, Shibaura Institute of Technology, Toyosu 3-7-5, Koto-ku, Tokyo 135-8548, Japan

R. Mizoguchi, A. Ishii
Department of Chemistry and Biochemistry, School of Advanced Science and Engineering, Waseda University, Okubo 3-4-1, Shinjuku-ku, Tokyo 169-8555, Japan

J. P. Hill
International Center for Materials Nanoarchitechtonics, National Institute for Materials Science, Namiki 1-1, Tsukuba, Ibaraki 305-0044, Japan
E-mail: jonathan.hill@nims.go.jp

Additional supporting information can be found online in the Supporting Information section

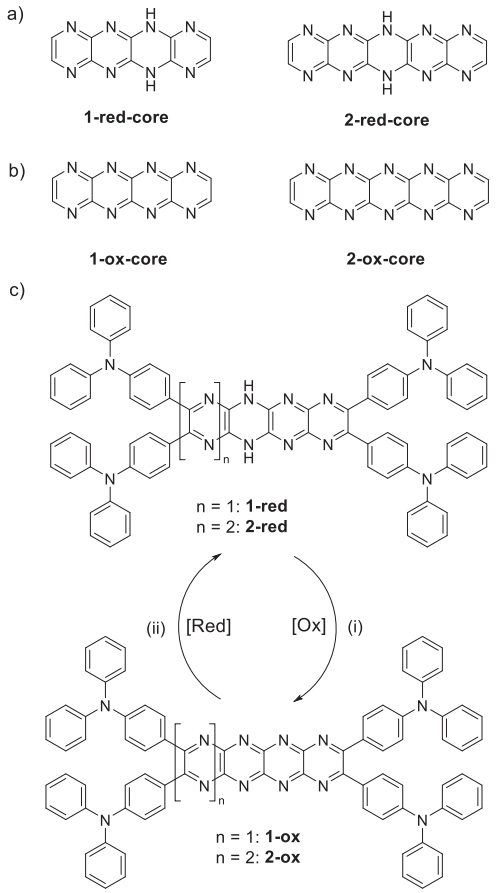

Scheme 1. Structures of unsubstituted a) reduced pyrazinacenes and b) pyrazinacenes in their fully oxidized state with no dihydropyrazine units. These core structures of **1** and **2** were used for DFT studies and demonstrated variation in electron-accepting capacity during the redox process. c) Structures of reduced species **1-red** and **2-red** and redox interconversion between the reduced and fully oxidized species **1-ox** and **2-ox** (i) PbO_2, $CHCl_3$; (ii) sodium dithionite (aq), $CHCl_3$.

bands well within the visible region. Higher pyrazinacenes having 6 or 7 pyrazine units, while showing fluorescence bands approaching the NIR region, always contain a dihydropyrazine unit and are stable against oxidation.[32,35] To create redox-active chromophores with absorption and fluorescence bands well into the NIR region, another strategy is needed. Intramolecular charge transfer (ICT) has been widely investigated as a means to reduce the optical energy gap in organic conjugated materials. The typical strategy involves linking electron donor (D) and acceptor (A) groups through a conjugated π-bridge which results in a lowering of the optical energy gap through ICT interactions. It is known that pyrazinacenes consisting of three or more fused pyrazine rings all in their fully oxidized state are extremely electron-deficient[32,34] and therefore should act as strong acceptors when combined with appropriate donor groups. Here, we describe a new series of compounds based on the redox-active octaazatetracene (**1**) and decaazapentacene (**2**) chromophores appended with electron-donating triphenylamine (TPA) groups (Scheme 1c) and investigate their redox-coupled photophysical properties.

Results and Discussion

Synthesis and Characterization

Synthesis of the D-A-D type compounds **1** and **2** was achieved through the condensation of a TPA-appended pyrazinopyrazine-2,3-dicarbonitrile with a TPA-appended diaminopyrazine (**S2**) for **1-red** as shown in Scheme 2 or diamino-pyrazinopyrazine (**S4**) for **2-red** as shown in Scheme S1. Compounds were isolated in the expected reduced form with a single dihydropyrazine unit occupying the central pyrazine unit of the pyrazinacene backbone. Typically, a reaction mixture of 5,6-bis(4-diphenylamino)phenylpyrazine-2,3-diamine and 6,7-bis(4-(diphenylamino)phenyl)pyrazino[2,3-*b*]pyrazine-2,3-dicarbonitrile in DMF in the presence of sodium bicarbonate was stirred for 2 h at 120 °C to yield the reduced compound **1-red**, which was purified by column chromatography (Yield: 48 %). **2-red** is obtained using a similar procedure with minor modifications to increase yield. Although oxidation of the compounds to **1-ox** and **2-ox** can be performed using different oxidants (e.g., 2,3-dichloro-5,6-dicyano-1,4-benzoquinone (DDQ), sodium hypochlorite), for convenience, lead (IV) oxide (PbO_2) suspended in $CHCl_3$ was selected as the oxidizing system because the oxidant can be separated by simple filtration. PbO_2 was added to a solution of **1-red** in $CHCl_3$. After completion, PbO_2 was filtered and the solvent was removed by evaporation. Purification by column chromatography yielded a dark green powder of **1-ox** in quantitative yield. The molecular structures of **1** and **2** were fully characterized using NMR, FTIR, and HRMS studies (Figures S1–S32); the dihydropyrazine protons were observed at $\delta = 7.77$ and 8.70 for **1-red** and **2-red**, respectively, and ionization peaks were found at 1211.4974 *m/z* for **1-red** (calcd. as $[C_{82}H_{59}N_{12}]^+$ $[M + H]^+$: 1211.4986 *m/z*), 1263.5022 *m/z* for **2-red** (calcd. as $[C_{84}H_{59}N_{14}]^+$ $[M + H]^+$ 1263.5047 *m/z*), respectively. Electron-donating TPA substituents are expected to stabilize the oxidized states by transfer of electron density to the highly electron-deficient pyrazinacene (i.e., **1-ox**/**2-ox**). The bulky TPA groups impart good solubility to these compounds such that they are readily soluble in low to moderately polar solvents such as toluene, tetrahydrofuran, and $CHCl_3$. Also, the attachment of TPA groups at the terminal carbon atoms of the pyrazinacene rather than as *N*-substituents of the dihydropyrazine unit allows the study of protic processes such as deprotonation, and importantly here, redox properties.

Green prismatic crystals of **1-ox**·4$CHCl_3$ suitable for X-ray crystallographic studies were obtained by slow evaporation of a $CHCl_3$ solution (Figure 1) revealing several interesting properties of the compound in the solid state. No electron densities, suggestive of hydrogen atoms characteristic of the reduced form, were observed around the pyrazine nitrogen atoms.

The TPA groups do not appear to be affected by the oxidation process as they possess the classic neutral TPA propeller shape. Oxidized TPAs are typically planarized by oxidation and are usually only stable when appropriately substituted.[37] Thus, the oxidation process only appears to

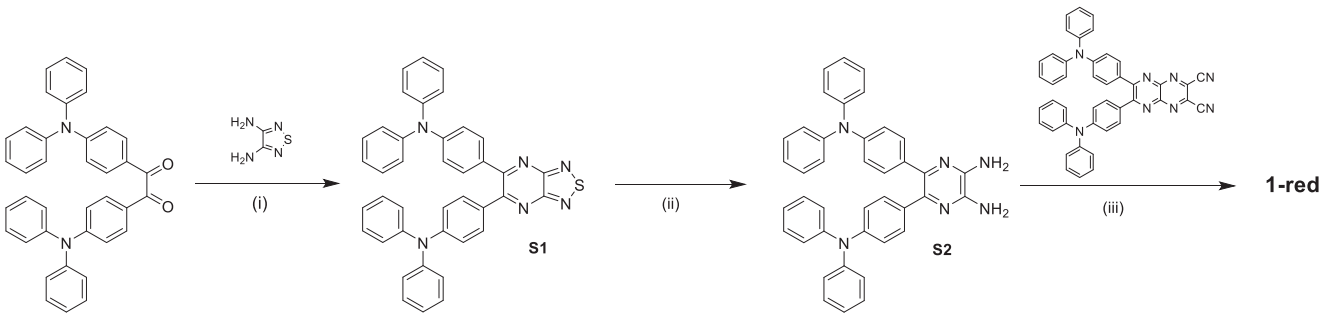

Scheme 2. Synthesis of **1-red**. (i) *p*-Toluenesulfonic acid, toluene, reflux; (ii) sodium dithionite, AcOH, 100 °C; (iii) sodium bicarbonate, DMF, 120 °C.

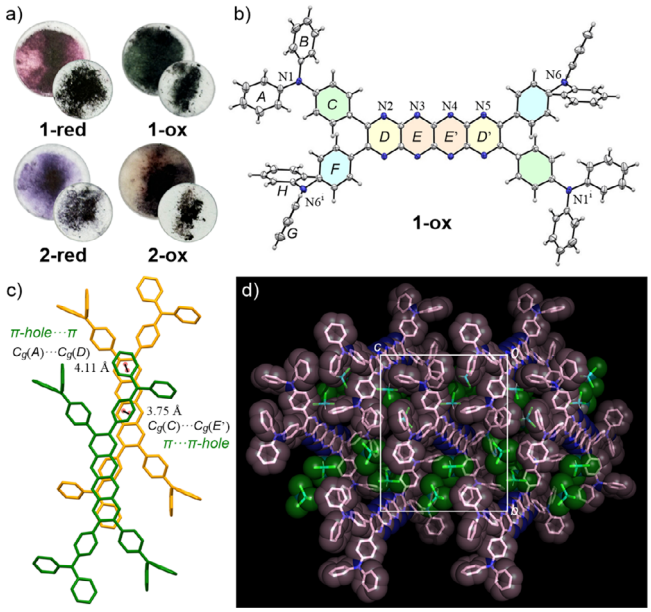

Figure 1. a) Appearances of solid samples of **1** and **2** with and without dispersion in $CHCl_3$. Crystal structure of **1-ox**·4$CHCl_3$ (CCDC2381770): b) ORTEP view of **1-ox** with 50 % thermal ellipsoids, c) intermolecular association showing $\pi\cdots\pi$-hole interactions between the electron donor TPA units and electron acceptor pyrazinacene units, and d) packing structure viewed along the *a*-axis; color schemes: **1-ox**, pink; $CHCl_3$, green.

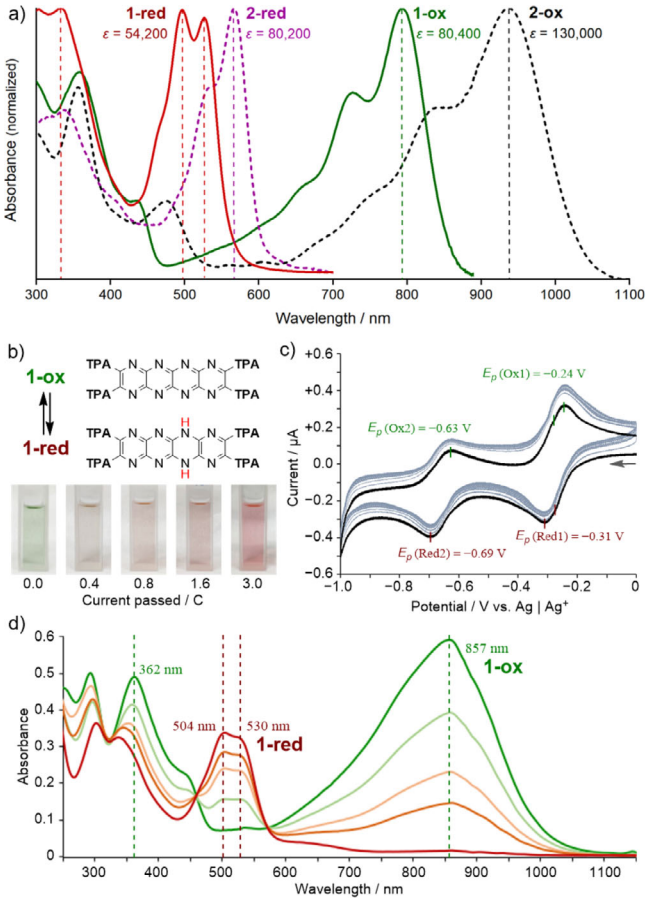

Figure 2. a) UV–vis–NIR absorption spectra of both states of **1** and **2** in CCl_4 solution with extinction coefficients, ε_{max} /M^{-1} cm^{-1}. b) Reversible color changes observed under constant current electrolysis, c) repeated CV (scan rate = 50 mV s^{-1}), and d) UV–vis–NIR absorption spectra under constant current electrolysis of **1-ox**/**1-red** in CH_2Cl_2. Constant current electrolysis was performed on a 2 × 10^{-4} M solution of **1-ox** with aliquots diluted to 1 × 10^{-5} M for UV–vis–NIR absorption measurements.

affect the pyrazinacene cores. The dihedral angle between rings *D* and *E* is 8.66°, with the torsion angle subtended between planes of the core (ring-*D*) and the two TPA substituents at 15.9(5)°, indicating that the bulky TPA substituents are responsible for a slightly twisted form of the pyrazinacene unit. Pyrazinacene and TPA sites are stacked in the structure indicating a π-hole$\cdots\pi$ interaction with the electron-deficient pyrazinacene moiety as an acceptor and the electron-rich TPA as a donor unit.

Redox-Coupled Photophysical Properties

Essential absorption properties of compounds **1** and **2** are summarized in Figure 2, Figures S33, S34. Compound **1-red** has absorption maxima (λ_{max}) in the range of 500–520 nm in most solvents (Figure 2a and Table 1). In CCl_4, its spectrum shows an acene-like vibronic structure with broadened peaks.

Compound **2-red** behaves similarly but with λ_{max} undergoing a bathochromic shift to 566 nm in CCl_4 due to the additional fused pyrazine unit. For **1-ox**, λ_{max} shifts from 527 nm (ε_{max} = 54000 M^{-1} cm^{-1}, red solid line in Figure 2a) to

Table 1: Photophysical properties of **1** and **2**. Maximum absorption wavelengths (λ_{abs}) in cyclohexane (C_6H_{12}), CCl_4, toluene, CH_2Cl_2, $CHCl_3$, and CH_3CN along with maximum emission wavelengths (λ_{em}) in the exemplary solvent CCl_4 are shown. Excitation wavelengths (λ_{ex}) are given in parentheses.

Compound	λ_{abs}/nm C_6H_{12}	λ_{abs}/nm CCl_4	λ_{abs}/nm toluene	λ_{abs}/nm CH_2Cl_2	λ_{abs}/nm $CHCl_3$	λ_{abs}/nm CH_3CN	λ_{em}/nm (λ_{ex}/nm) CCl_4	Φ_{PL} CCl_4
1-red	507	497, 527	495, 523	503, 523	512, 533	493, 515	560 (496)	0.58
1-ox	795	793	731, 793	829	879	802	847 (700)[a]	0.16
2-red	538, 572	536, 566	525, 560	715	586	548	599 (535)	0.43
2-ox	907	836, 937	840[b], 927	1042	1051	965	1012 (700)[a]	0.014

[a] Compounds were excited at the maximum absorption wavelength except for oxidized species **1-ox** and **2-ox** which were excited at 700 nm due to an instrumental limitation. [b] Shoulder absorption.

793 nm ($\varepsilon_{max} = 80400\ M^{-1}\ cm^{-1}$, green solid line in Figure 2a) – a 266 nm bathochromic shift. For **2-ox** a bathochromic shift of 371 nm is observed in CCl_4 with λ_{max} shifting from 566 nm ($\varepsilon_{max} = 80200\ M^{-1}\ cm^{-1}$, violet dashed line in Figure 2a) to 937 nm ($\varepsilon_{max} = 130000\ M^{-1}\ cm^{-1}$, black dashed line in Figure 2a).

We conducted electrochemical analyses to further investigate the reversibility of the redox processes of the compounds (Figure 2b–d). A green solution of **1-ox** (2×10^{-4} M CH_2Cl_2/CH_3OH and electrolyte Bu_4NBF_4) was used to perform cyclic voltammetry (CV) and constant current electrolysis. The first and second reversible reduction waves were found respectively at −0.28 V ($\Delta E = 70$ mV) and −0.66 V ($\Delta E = 60$ mV) with good reversibility even after several cycles, as shown in Figure 2c. The first reduction wave consists of two overlapping peaks suggesting, together with results of previous reports and DFT calculations, that the central pyrazine (ring-*E*) is reduced. Attempts to isolate reduction products using constant potential electrolysis proved unsuccessful, possibly due to low current issues. However, we note that the electrochemical reduction of structurally similar azaacenes in the presence of a proton source, including quinoxalino[2,3-*b*]quinoxaline and pyrazino[2,3-*b*]quinoxaline, typically results in successive $2e^-$, $2H^+$ processes corresponding to reduction of pyrazine units directly to 1,4-dihydropyrazine units.[38,39] This is consistent with our findings using constant current electrolysis, during which the solution color and spectra (with a clear isosbestic point–Figure 2d) indicate conversion of **1-ox** directly to its reduced state **1-red** without the involvement of any stable intermediate species.

The reversibility of the chemical redox process was confirmed through successive chemical redox transformations between oxidized and reduced species. PbO_2 was added to a solution of as-synthesized **1-red** in tetrachloroethane-d_2 or **2-red** in $CDCl_3$ and after stirring for 3 min, the mixture was filtered before ^1H NMR analysis of the filtrate, which confirmed conversion to the oxidized species as evidenced by the distinctive large downfield shift of the aromatic hydrogen resonances immediately adjacent to the pyrazinacene cores. Reduction was achieved by adding an aqueous solution of sodium dithionite and the biphasic mixture was stirred for 3 min before solvent partitioning and washing the organic layer with brine before ^1H NMR analysis which confirmed conversion back to the reduced species. The same oxidation and reduction processes were repeated several times, and the

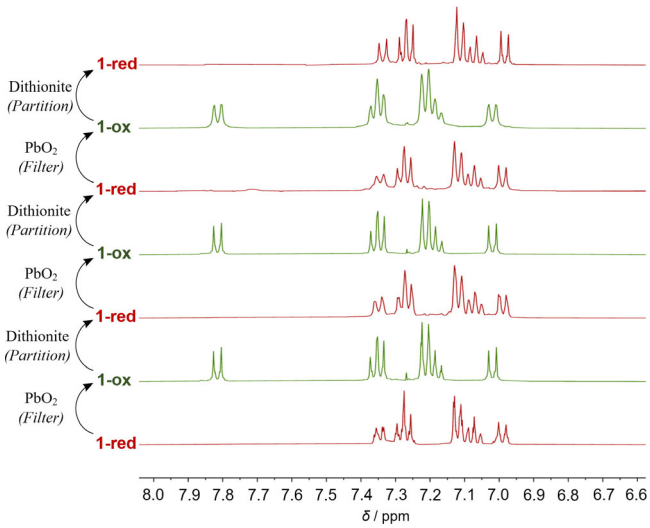

Figure 3. ^1H NMR spectra, starting with as-synthesized **1-red** showing successive chemical redox transformations between **1-red** and **1-ox**. Remarkably, all redox steps were performed without the necessity of further purification beyond filtration of the PbO_2 oxidant and solvent partitioning of the aqueous dithionite reducing agent demonstrating smooth, quantitative chemical conversions between the two species.

results are shown in Figure 3 and Figure S35 demonstrating the repeatability of the chemical redox process.

The reduced species exhibit fluorescence in solution with moderate to high photoluminescence quantum yields (PLQY, Φ_{PL}) as shown in Figure 4 and Table 1. Compound **1-red** in CCl_4 exhibits fluorescence at $\lambda_{em} = 560$ nm with a PLQY $\Phi_{PL} = 0.58$. Compound **2-red** shows similar fluorescence properties but with a $\Phi_{PL} = 0.43$ and a bathochromically shifted $\lambda_{em} = 599$ nm. **1-red** and **2-red** exhibit vivid yellow and red luminescence, respectively, as shown in Figure 4a. In low-polarity solvents, such as CCl_4, cyclohexane, or toluene, NIR fluorescence is also observed for both oxidized species. For **1-ox**, $\lambda_{em} = 847$ nm in CCl_4 while for compound **2-ox**, fluorescence extends to the SWIR region (1000–1700 nm) with $\lambda_{em} = 1012$ nm. Note that the excitation wavelength λ_{ex} in both cases was 700 nm due to an instrumental limitation, although values of PLQY obtained are sufficiently high to consider applications of the materials.

As expected for NIR emitters, fluorescence quantum yields of the oxidized species are significantly diminished compared to their reduced counterparts due to increased

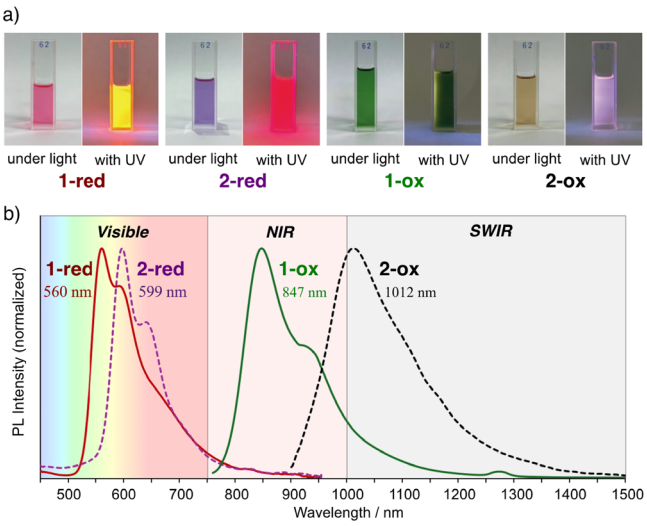

Figure 4. a) Appearance of CCl_4 solutions of **1** and **2** under visible light and UV illumination (365 nm) and b) emission spectra of **1** and **2** in CCl_4 showing the extreme shift in fluorescence wavelengths between reduced and oxidized species.

rates of non-radiative processes, which for NIR and SWIR emitters are typically dominated by non-adiabatic coupling between excited and ground electronic states.[40] Nonetheless, the fluorescence quantum yields compare well with some of the highest reported values for organic NIR and SWIR fluorophores[41] with compound **1-ox** showing a PLQY of 16.4 % with a brightness of 13200 M^{-1} cm^{-1} (SWIR brightness = 1690 M^{-1} cm^{-1}) and **2-ox** showing a PLQY of 1.4 % with a brightness of 1810 M^{-1} cm^{-1} (SWIR brightness = 1370 M^{-1} cm^{-1}) in CCl_4.

Computational Studies and Discussion

Electronic absorption spectra of the compounds were predicted using Time-Dependant Density Functional Theory (TDDFT B3LYP def2-TZVP) including a conductor-like polarizable continuum solvent model (CPCM) for CCl_4 as implemented in the Orca 6.0.0 software package[42] and are shown in Figure 5.

The large redox-coupled shifts in absorption peaks were predicted remarkably well, albeit with peaks somewhat bathochromically shifted compared to experimental values. For **1-red** the longest wavelength absorption peak was calculated at λ_{abs} = 608 nm (*c.f.* measured λ_{abs} = 527 nm). For **1-ox** the longest wavelength absorption was calculated at λ_{abs} = 938 nm (*c.f.* measured λ_{abs} = 793 nm). For **2-red** the longest wavelength absorption was calculated at λ_{abs} = 648 nm (*c.f.* measured λ_{abs} = 566 nm). For **2-ox** the longest wavelength absorption was calculated at λ_{abs} = 1078 nm (*c.f.* measured λ_{abs} = 937 nm). All calculated longest wavelength absorptions were due to simple highest occupied to lowest unoccupied molecular orbital (HOMO-LUMO) singlet ($S_0 \rightarrow S_1$) transitions.

Oxidation of the pyrazinacene cores results in a significant deepening in the energy of the LUMO of the core units.

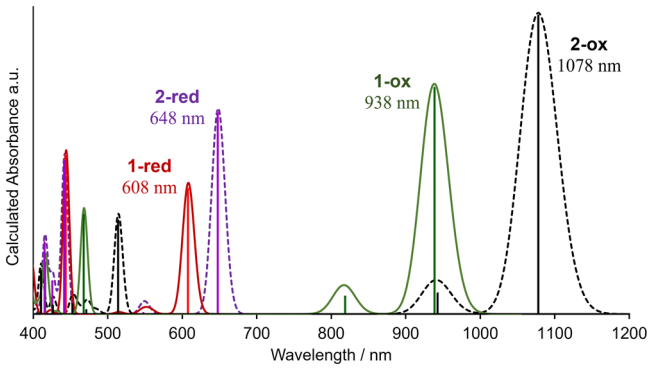

Figure 5. Calculated UV–vis–NIR absorption spectra for compounds **1** and **2** using the TDDFT B3LYP def2-TZVP method with CPCM (CCl_4) solvent model. Artificial spectra are created by broadening calculated transitions by 500 cm^{-1} at full-width-half-maximum (FWHM) and scaling vertically according to the oscillator strength. The main calculated transitions are shown by vertical solid lines.

DFT modeling (B3LYP 6–311 + G**) shows a LUMO energy level, E_{LUMO} = −2.68 eV for **1-red-core** which decreases to −4.56 eV upon oxidation to **1-ox-core** (Figures S40,S41). Similarly, **2-red-core** has a calculated E_{LUMO} = −3.24 eV which decreases to −4.99 eV in the fully oxidized species **2-ox-core** (Figures S42,S43). This latter value is comparable with that of the strongly electron-accepting 2,5-difluoro-7,7,8,8-tetracyanoquinodimethane (E_{LUMO} = −4.6 eV).[43] Thus, the driving force for the large shift in photophysical properties observed after oxidation is due to a change from D-A-D type structures having weak-to-moderate acceptor units in **1-red** and **2-red** to D-A-D type structures containing exceptionally strong electron acceptor units in **1-ox** and **2-ox**. Nitrogen atoms can act as either electron donors or acceptors when incorporated into a π-system depending on the orientation of the nitrogen lone pair electrons. When the nitrogen lone pair electrons are oriented orthogonally to the π-system such as the sp^2 hybridized nitrogen atoms of pyrazine, the lone pair electrons cannot overlap with and donate into the π-system efficiently and the strongly electronegative nitrogen atoms withdraw electron density from the π-system inductively. Conversely, the lone pair electrons of sp^3 hybridized nitrogen atoms pendant to a π-system, such as those in TPA, can overlap with and donate to the π-system and the nitrogen atoms act as electron donors. The nitrogen atoms of the reduced 1,4-dihydropyrazine ring can be regarded as a special case of the latter in which the lone pair electrons are fully donated into the π-system to give a planarized, electron-rich anti-aromatic system in which the anti-aromaticity is stabilized through delocalization across the π-system.[44,45] The molecules described in this manuscript take advantage of all three of these effects to achieve extreme redox-coupled shifts in absorption and fluorescence. To gain further insight into the changes in donor and acceptor strength of the TPA groups and pyrazinacene cores across the redox process, the electrostatic potential (ESP) energy surfaces were simulated (Figures S44–S47). Strongly negative ESP values were found at the centers of TPA phenyl groups (−42.5 to −65.4 kJ mol^{-1}) indicating the electron-rich character of the donor groups.

Strongly positive ESP values (+24.9 to +121.6 kJ mol^{-1}) were found at the centers of the pyrazinacene rings indicating the electron-deficient character of the acceptor units. An increase in the ESP values at the centers of the TPA phenyl groups occurs upon oxidation of the compounds suggesting there is some transfer of electron density from the TPA groups to the more electron-deficient pyrazinacene cores in the oxidized species. Changes to the ESP values on the pyrazinacene cores between oxidized and reduced species are less consistent, possibly due to the structural changes involved as well as significant contributions from the nitrogen lone pair electrons. Inspection of the frontier orbital locations and changes in their energy levels during the redox process provides more detailed insight into the redox-coupled changes in photophysical properties observed in the present compounds. In these D-A-D type structures, the HOMO lies predominantly on the TPA donor units (Figures S36–S39) and is largely unperturbed by the redox process (**1-red** $E_{HOMO} = -5.2$ eV, **1-ox** $E_{HOMO} = -5.3$ eV; **2-red** $E_{HOMO} = -5.2$ eV, **2-ox** $E_{HOMO} = -5.4$ eV). The LUMOs in all species are located predominantly on the pyrazinacene cores and are strongly perturbed by the redox process (**1-red** $E_{LUMO} = -2.8$ eV, **1-ox** $E_{LUMO} = -3.6$ eV; **2-red** $E_{LUMO} = -2.8$ eV, **2-ox** $E_{LUMO} = -3.9$ eV). The stabilization of the LUMO energy levels together with the only minor variations in the HOMO energy levels upon oxidation leads to a significant narrowing of the energy gap and so a large bathochromic shift in absorption/fluorescence is realized. This contrasts significantly with our previously reported redox-active pyrazinacenes[34,36] whose HOMOs and LUMOs are both located on the pyrazinacene cores and are thus both perturbed to a similar extent by the redox process so that large shifts in the optical energy gaps are not observed.

For many organic NIR emitters, high-frequency C─H vibrational modes make a significant contribution to the non-radiative relaxation rate due to a large overlap integral between ground and excited states.[46] A strategy to improve NIR fluorescence quantum yields has involved the substitution of hydrogen atoms with heavier deuterium or fluorine atoms to reduce the frequency of vibrational modes.[46,47] This strategy, however, can be synthetically challenging and for more complex molecules, not economically viable due to the high cost of deuterated synthesis intermediates. Our molecular design strategy incorporates the strong acceptors octaazatetracene and decaazapentacene as major components of their π-conjugated systems and eliminates adjacent C─H bonds, which is expected to reduce the non-radiative decay rates. As the molecules reported here are the first examples using this strategy, we anticipate further improvements in NIR fluorescence quantum yields could be realized, especially through tuning of the donor structures.

Conclusion

In conclusion, we present a strategy for the synthesis of organic chromophores based on the octaazatetracene and decaazapentacene pyrazinacene cores appended with TPA electron donor groups. To achieve efficient fluorescence in the NIR and SWIR regions, these compounds incorporate fully oxidized pyrazinacenes as a significant component of the chromophore. This component contains no C─H or N─H bonds whose high-frequency vibrational modes would strongly contribute to non-radiative decay above 850 nm, as is found in most organic compounds.[46] Replacement of C─H units with nitrogen atoms demonstrates an alternative to existing strategies relying on deuterium or fluorine substitution to achieve higher NIR fluorescence quantum yields. The molecules described herein have a D-A-D quadrupolar type motif with the pyrazinacene forming a strong acceptor and a large part of the π-conjugated system. However, there is no reason why fully oxidized pyrazinacenes cannot be used in other structures commonly used in long wavelength emitters, such as D-A dipolar, anionic, cationic, or zwitterionic motifs. The chromophores described herein have fluorescence quantum yields that compare well with some of the best-known chromophores at these wavelengths and we anticipate that by tuning the donor structures, it will be possible to further increase fluorescence quantum yields. Additionally, these compounds can be easily switched using a simple, reversible redox process between highly fluorescent reduced states with absorption and emission in the visible region (λ_{em} = 560 nm for **1-red** and λ_{em} = 599 nm for **2-red** in CCl_4) to oxidized states having absorption and emission bands in the NIR (λ_{em} = 847 nm for **1-ox**) or even SWIR (λ_{em} = 1012 nm for **2-ox**) regions. Such large shifts in photophysical properties are quite remarkable and unprecedented for a redox process that affects only a single, six-membered ring in which both reduced and oxidized states consist of neutral, closed-shell species. Redox switching can be achieved either electrochemically or by using different oxidizing and reducing agents including the biologically relevant oxidant hypochlorite and Hantzsch ester, a mimic of the biological reductant 1,4-dihydronicotinamide adenine dinucleotide (NADH). While these compounds currently lack water solubility for biological use, their redox properties suggest that water-compatible analogs could lead to a novel category of fluorescent probes for tracking redox processes in biological and cellular environments. The molecular design strategy showcased here should not only apply to a wide variety of electron-donor appended pyrazinacenes, but also to any ICT conjugated organic systems in which the acceptor units can be modified to incorporate a redox-active pyrazine/dihydropyrazine unit. Based on the results of this work, such materials can be expected to show similarly large redox-coupled changes in their photophysical properties that should be beneficial to a wide variety of applications.

Supporting Information

Details of synthetic procedures, crystal structural information, additional electronic absorption spectra, and DFT calculations are provided in the supporting information. Deposition number 2381770 contains the supplementary crystallographic data for this paper. These data are provided free of charge by the joint Cambridge Crystallographic Data Center and Fachinformationszentrum Karlsruhe

Access Structures service. The authors have cited additional references within the Supporting Information.[48–51]

Acknowledgements

This work was supported by Grants-in-Aid for Scientific Research C, no. 21K05044 and 24K08401 (G.J.R.) and parts of this work was supported by Grant-in-Aids for Scientific Research B, no. 21H01955 and 23K21122 (A.H.) of JSPS KAKENHI and by World Premier International Research Center Initiative (WPI Initiative), MEXT, Japan (J.P.H.).

Conflict of Interests

The authors declare no conflict of interest.

Data Availability Statement

The data that support the findings of this study are available in the supplementary material of this article.

Keywords: Fluorescent probes · NIR absorption · NIR fluorescence · Pyrazinacenes · Redox-active dyes

[1] Z. Guo, S. Park, J. Yoon, I. Shin, *Chem. Soc. Rev.* **2014**, *43*, 16–29.
[2] C. Liu, S. Zhang, J. Li, J. Wei, K. Müllen, M. Yin, *Angew. Chem., Int. Ed.* **2019**, *58*, 1638–1642.
[3] Y. Chen, S. Wang, F. Zhang, *Nat. Rev. Bioeng.* **2023**, *1*, 60–78.
[4] J. Mu, M. Xiao, Y. Shi, X. Geng, H. Li, Y. Yin, X. Chen, *Angew. Chem., Int. Ed.* **2022**, *61*, e202114722.
[5] P. L. dos Santos, P. Stachelek, Y. Takeda, P. Pander, *Mater. Chem. Front.* **2024**, *8*, 1731–1766.
[6] Y. Xiao, H. Wang, Z. Xie, M. Shen, R. Huang, Y. Miao, G. Liu, T. Yu, W. Huang, *Chem. Sci.* **2022**, *13*, 8906–8923.
[7] E. H. Cho, H.-R. Choi, Y. Park, S. Y. Jeong, Y. J. Song, Y. H. Hwang, J. Lee, Y. Chi, S.-F. Wang, Y. Jeon, C.-H. Huh, K. C. Choi, *ACS Appl. Mater. Interfaces* **2023**, *15*, 57415–57426.
[8] S. I. Reja, M. Minoshima, Y. Hori, K. Kikuchi, *Chem. Sci.* **2021**, *12*, 3437–3447.
[9] C. Canovas, P.-S. Bellaye, M. Moreau, A. Romieu, F. Denat, V. Goncalves, *Org. Biomol. Chem.* **2018**, *16*, 8831–8836.
[10] Q. Wu, M. Taki, Y. Tanaka, M. Kesherwani, Q. M. Phung, S. Enoki, Y. Okada, F. Tama, S. Yamaguchi, *Angew. Chem., Int. Ed.* **2024**, *63*, e202400711.
[11] H. Jiang, Y. Ren, W. Zhang, Y. Wu, E. C. Socie, B. I. Carlsen, J.-E. Moser, H. Tian, S. M. Zakeeruddin, W.-H. Zhu, M. Grätzel, *Angew. Chem., Int. Ed.* **2020**, *59*, 9324–9329.
[12] J. Watson, R. R. Rodrigues, J. H. Delcamp, *Cell Rep. Phys. Sci.* **2022**, *3*, 100701.
[13] A. Singh, A. K. Singh, R. Dixit, K. Vanka, K. Krishnamoorthy, J. Nithyanandhan, *ACS Appl. Energy Mater.* **2024**, *7*, 1461–1475.
[14] X. Zhang, Y. Wu, L. Chen, J. Song, H. Yang, *Chem. Biomed. Imag.* **2023**, *1*, 99–109.
[15] D. Jung, S. Park, C. Lee, H. Kim, *Polymers* **2019**, *11*, 1693.
[16] D. Y. Lee, J. Y. Kim, Y. Lee, S. Lee, W. Miao, H. S. Kim, J.-J. Min, S. Jon, *Angew. Chem., Int. Ed.* **2017**, *56*, 13684–13688.
[17] T. Kololuoma, J. A. I. Oksanen, P. Raerinne, J. T. Rantala, *J. Mater. Res.* **2001**, *16*, 2186–2188.
[18] G. Zhao, Y. Feng, S. Guang, H. Xu, N. Lin, X. Liu, *RSC Adv.* **2017**, *7*, 53785–53796.
[19] H. Khandelwal, A. P. H. J. Schenning, M. G. Debije, *Adv. Energy Mater.* **2017**, *7*, 1602209.
[20] M. Han, B. Kim, H. Lim, H. Jang, E. Kim, *Adv. Mater.* **2020**, *32*, 1905096.
[21] J. Volarić, W. Szymanski, N. A. Simeth, B. L. Feringa, *Chem. Soc. Rev.* **2021**, *50*, 12377–12449.
[22] P. Rietsch, S. Sobottka, K. Hoffmann, A. A. Popov, P. Hildebrandt, B. Sarkar, U. Resch-Genger, S. Eigler, *Chem.-Eur. J.* **2020**, *26*, 17361–17365.
[23] A. Muranaka, S. Ohira, D. Hashizume, H. Koshino, F. Kyotani, M. Hirayama, M. Uchiyama, *J. Am. Chem. Soc.* **2012**, *134*, 190–193.
[24] J. Huang, K. Pu, *Angew. Chem., Int. Ed.* **2020**, *59*, 11717–11731.
[25] J. Xuan, J. Yu, C. Huang, *ChemBioChem* **2024**, *25*, e202400467.
[26] C. Chen, R. Tian, Y. Zeng, C. Chu, G. Liu, *Bioconjugate Chem.* **2020**, *31*, 276–292.
[27] S. Yanagi, A. Matsumoto, N. Toriumi, Y. Tanaka, K. Miyamoto, A. Muranaka, M. Uchiyama, *Angew. Chem. Int. Ed.* **2023**, *62*, e202218358.
[28] Y. Koide, M. Kawaguchi, Y. Urano, K. Hanaoka, T. Komatsu, M. Abo, T. Terai, T. Nagano, *Chem. Commun.* **2012**, *48*, 3091–3093.
[29] L. He, L.-H. He, S. Xu, T.-B. Ren, X.-X. Zhang, Z.-J. Qin, X.-B. Zhang, L. Yuan, *Angew. Chem., Int. Ed.* **2022**, *61*, e202211409.
[30] N. S. James, R. R. Cheruku, J. R. Missert, U. Sunar, R. K. Pandey, *Molecules* **2018**, *23*, 1842.
[31] A. Bera, D. Bagchi, S. K. Pal, *J. Phys. Chem. A* **2019**, *123*, 7550–7557.
[32] G. J. Richards, J. P. Hill, *Acc. Chem. Res.* **2021**, *54*, 3228–3240.
[33] G. J. Richards, J. P. Hill, T. Mori, K. Ariga, *Org. Biomol. Chem.* **2011**, *9*, 5005–5017.
[34] G. J. Richards, J. P. Hill, N. K. Subbaiyan, F. D'Souza, P. A. Karr, M. R. J. Elsegood, S. J. Teat, T. Mori, K. Ariga, *J. Org. Chem.* **2009**, *74*, 8914–8923.
[35] G. J. Richards, A. Cador, S. Yamada, A. Middleton, W. A. Webre, J. Labuta, P. A. Karr, K. Ariga, F. D'Souza, S. Kahlal, J.-F. Halet, J. P. Hill, *J. Am. Chem. Soc.* **2019**, *141*, 19570–19574.
[36] D. Miklík, S. Fatemeh Mousavi, Z. Burešová, A. Middleton, Y. Matsushita, J. Labuta, A. Ahsan, L. Buimaga-Iarinca, P. A. Karr, F. Bureš, G. J. Richards, P. Švec, T. Mori, K. Ariga, Y. Wakayama, C. Morari, F. D'Souza, T. A. Jung, J. P. Hill, *Commun. Chem.* **2021**, *4*, 29.
[37] J. S. Wagner, M. A. Siegler, A. L. Tomlinson, J. R. Reynolds, *Adv. Opt. Mater.* **2024**, *12*, 2400855.
[38] J. Armand, L. Boulares, C. Bellec, J. Pinson, *Can. J. Chem.* **1982**, *60*, 2797–2803.
[39] J. Armand, L. Boulares, C. Bellec, J. Pinson, *Can. J. Chem.* **1987**, *65*, 1619–1623.
[40] R. Englman, J. Jortner, *Mol. Phys.* **1970**, *18*, 145–164.
[41] E. D. Cosco, B. A. Arús, A. L. Spearman, T. L. Atallah, I. Lim, O. S. Leland, J. R. Caram, T. S. Bischof, O. T. Bruns, E. M. Sletten, *J. Am. Chem. Soc.* **2021**, *143*, 6836–6846.
[42] F. Neese, *WIREs Comput. Mol. Sci.* **2022**, *12*, e1606.
[43] H. Méndez, G. Heimel, S. Winkler, J. Frisch, A. Opitz, K. Sauer, B. Wegner, M. Oehzelt, C. Röthel, S. Duhm, D. Többens, N. Koch, I. Salzmann, *Nat. Commun.* **2015**, *6*, 8560.
[44] S. Miao, S. M. Brombosz, P. v. R. Schleyer, J. I. Wu, S. Barlow, S. R. Marder, K. I. Hardcastle, U. H. F. Bunz, *J. Am. Chem. Soc.* **2008**, *130*, 7339–7344.
[45] J. I. Wu, C. S. Wannere, Y. Mo, P. v. R. Schleyer, U. H. F. Bunz, *J. Org. Chem.* **2009**, *74*, 4343–4349.
[46] S. F. Wang, B. K. Su, X. Q. Wang, Y. C. Wei, K. H. Kuo, C. H. Wang, S. H. Liu, L. S. Liao, W. Y. Hung, L. W. Fu, W. T. Chuang,

M. Qin, X. Lu, C. You, Y. Chi, P. T. Chou, *Nat. Photonics* **2022**, *16*, 843–850.
[47] H. C. Friedman, E. D. Cosco, T. L. Atallah, S. Jia, E. M. Sletten, J. R. Caram, *Chem* **2021**, *7*, 3359–3376.
[48] Z. Li, D. Yang, C. Han, B. Zhao, H. Wang, Y. Man, P. Ma, P. Chang, D. Ma, H. Xu, *Angew. Chem., Int. Ed.* **2021**, *60*, 14846–14851.
[49] B. Tang, J. Qi, M. Chem, W. Qin, P. Zhang, The Hong Kong University of Science and Technology, WO2018108070, **2018**.
[50] Z. Zhang, X. Du, S. Sviridov, G. Chopiuk, Novelion Therapeutics Inc, US6514972B2, **2002**.
[51] Y. C. Tong, Dow Chemical Co., US3987044 A, **1976**.

Manuscript received: February 25, 2025
Revised manuscript received: March 01, 2025
Accepted manuscript online: March 03, 2025
Version of record online: March 20, 2025